Measurements of the fluctuating pressure at the wall beneath a thick turbulent boundary layer

By W. W. WILLMARTH AND C. E. WOOLDRIDGE
Department of Aeronautical and Astronautical Engineering, The University of Michigan

(Received 24 April 1962)

Measurements of the turbulent pressure field at the wall beneath a thick (5-inch) turbulent boundary layer produced by natural transition on a smooth surface are reported. The data include the mean-square pressure, power spectrum of the pressure, space-time correlation of the pressure parallel to the stream, and spatial correlation of the pressure transverse to the stream.

The root-mean-square wall pressure was 2·19 times the wall shear stress. The power spectra of the pressure were found to scale with the free-stream speed and the boundary-layer displacement thickness. A few tests with a rough surface showed that the increase in root-mean-square wall pressure was greater than the increase in wall shear stress.

The space-time correlation measurements parallel to the stream direction exhibit maxima at certain time delays corresponding to the convection of pressure-producing eddies at speeds varying from 0·56 to 0·83 times the stream speed. The lower convection speeds are measured when the spatial separation of the pressure transducers is small, or when only the pressure fluctuations at high frequencies are correlated. Higher convection speeds are observed when the spatial separation of the pressure transducers is large, or when only low frequencies are correlated. The result that low-frequency pressure fluctuations have the highest convection speed is in agreement with the measurements of Corcos (1959, 1962) in a fully turbulent tube flow. Analysis of these measurements also shows that both large- and small-scale pressure-producing eddies decay after travelling a distance proportional to their scale. More precisely, a pressure-producing eddy of large or small wavelength λ decays and vanishes after travelling a distance of approximately 6λ.

The transverse spatial correlation of the wall-pressure fluctuations was measured and compared with the longitudinal scale. Both the transverse and the longitudinal scale of the pressure fluctuations were of the order of the boundary-layer displacement thickness. The transverse and longitudinal scales of both large- and small-scale wall-pressure fluctuations were also measured and were also found to be approximately the same.

1. Introduction

Knowledge of the pressure fluctuations within a turbulent boundary layer is desired for many problems in fluid mechanics. One of these is the aerodynamic noise produced by turbulence in the boundary layer adjacent to a rigid surface.

Another type of problem arises when a turbulent boundary layer is developed adjacent to a flexible surface, and the pressure fluctuations can cause motion of the surface normal to itself. The questions of wave generation on liquid surfaces, sound generation by motion of thin membranes or plates, and turbulence inhibition by surface motion are then of interest. In addition, knowledge of the turbulent pressure fluctuations may lead to a better understanding of the structure of the turbulent boundary layer.

The first theoretical and experimental studies of turbulent pressure fluctuations were concerned with isotropic turbulence. The papers of Batchelor (1950) and Uberoi (1953) represent relatively recent contributions to the theoretical and experimental literature and give historical reviews of the problem. In the boundary layer one is faced with the much more difficult problem of pressure fluctuations in anisotropic turbulence developed along a wall. Kraichman (1956*a*, *b*) has shown that the primary contribution to the pressure fluctuations in the boundary layer near the wall must be attributed to the interaction of the turbulence with mean shear. He estimated (1956*b*) that the magnitude of the root-mean-square pressure fluctuations at the wall were of the order of the wall shear stress. Confirmation of this estimate and additional information about the wall-pressure fluctuations has had to be obtained experimentally.

Direct measurements of pressure fluctuations within a turbulent flow are not possible because a suitable pressure transducer, free from interaction with the turbulent flow, does not exist. Uberoi (1953) avoided the problem of direct pressure measurement by use of the fact that hot-wire measurements of a certain few velocity correlations, in isotropic turbulence, can be used to compute pressure correlations. In the work reported here, the pressure fluctuations on the wall beneath the turbulent boundary layer were measured directly with a pressure transducer flush with the surface.

Experimental measurements of the wall-pressure fluctuations beneath various turbulent shear flows have already been reported: beneath turbulent boundary layers by Harrison (1958), Willmarth (1958*a*, 1959), and Bull (1960) at subsonic speeds, and Kistler (portions of his results having been reported by Laufer 1961) at both subsonic and supersonic speeds; in a fully developed turbulent flow in a tube by Corcos (1962); and beneath a wall jet by Lilley & Hodgson (1960). All investigators report measurements of the spectrum of the pressure and the space-time correlation of the pressure. The correlation measurements show that the pressure fluctuations are convected downstream at approximately $0{\cdot}8U_\infty$ and decay after travelling a few boundary-layer thicknesses.

Very little additional information exists about the fine structure of the wall-pressure fluctuations, primarily because the previous investigations were made with pressure transducers that, compared to the boundary-layer thickness, were relatively large. The present experiments beneath a thick turbulent boundary layer were devised in an attempt to increase the precision of the existing experimental information and to learn more about the detailed structure of the wall-pressure fluctuations. We are also investigating the correlation between the wall pressure and the velocity components in the boundary layer to learn more about the structure and scale of the eddies that produce the pressure fluctua-

tions. The pressure-velocity correlation measurements will be reported in a later paper.

After this paper had been written the authors received a paper reporting the recent measurements of longitudinal space-time correlation and spectra of the wall pressure in a water tunnel by Bull & Willis (1961). Their measurements arrived too late to be compared in detail with ours, but it can be stated that their work is in agreement with ours on the essential points. They also find an increasing convection velocity with increasing transducer spacing

$$(0{\cdot}7 < U_c/U_\infty < 0{\cdot}85),$$

and they find $\sqrt{(\overline{p^2})^{\frac{1}{2}}}/\tau_w \simeq 2{\cdot}7$.

2. Experimental procedure

2.1. *Experimental equipment*

The measurements were made on the floor of the 5×7 ft. test section of The University of Michigan's subsonic wind tunnel. The wind-tunnel test section is 25 ft. long and is indoors. The settling chamber, fan, and steel ducting that

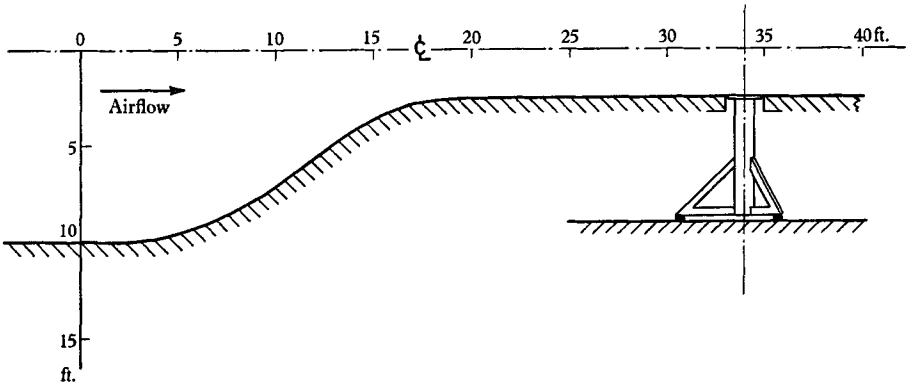

FIGURE 1. Scale drawing of wind-tunnel test section and massive vibration isolation mounting for the pressure transducers.

recirculates the air are out of doors. The total distance around the wind-tunnel circuit is 332 ft. The contraction ratio of the nozzle is 15 : 1.

The pressure measurements were made on the surface of a smooth (oil-lapped) steel disk, of 1 in. thickness and 20 in. diameter, that was sealed against air leaks and inset flush with the floor of the test section. Holes were drilled through the disk to allow insertion of pressure transducers or of dummy transducers (brass plugs). The plugs and transducers were always flush with the surface within $\pm 0{\cdot}001$ in. A special test established that $\pm 0{\cdot}001$ in. misalignment produced less than 1 % increase in the root-mean-square wall pressure. The steel disk was welded to a hollow steel tube that was filled with sand and fitted with legs and alignment jacks. This massive 800 lb. assembly was partially isolated from the vibrations of the concrete floor of the laboratory by thick rubber pads. Figure 1 is a sketch of the plate mounted in the wind-tunnel floor.

The fluctuating wall pressure was detected by lead-zirconate pressure transducers. The transducer dimensions and construction were identical with those

of the barium-titanate transducers already developed and reported by Willmarth (1958*b*). The diameter of the sensitive area of the transducer was 0·163 in. The frequency response of the transducers was uniform in the frequency range of interest, 20–10,000 c/s. The pressure-transducer sensitivity was determined by placing the transducers in a closed volume and varying the volume with a piston driven by a connecting rod and crankshaft. Assuming an isentropic compression or expansion, the pressure change was computed from the known volume change.

The transducer response to pressure fluctuations whose length scale (say half the wavelength) is of the order of the diameter of the sensitive area of the transducer or greater will not suffer serious cancellation effects. The ratio of transducer diameter, 0·163 in., to boundary-layer thickness, 5 in., was approximately 1 : 30. Thus we may expect that measurements of pressure fluctuations for which a half wavelength is greater than $\frac{1}{30}$th of the boundary-layer thickness will not be seriously affected by the transducer size.

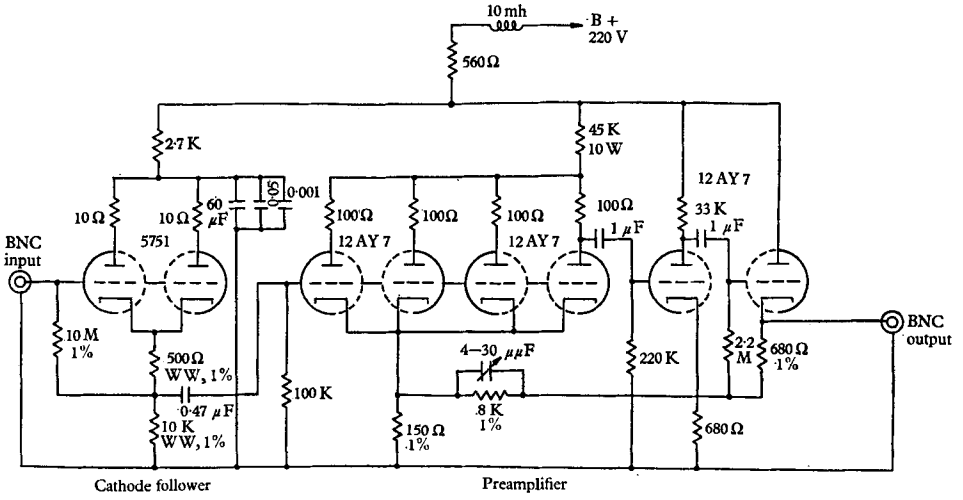

FIGURE 2. Circuit diagram for high-input-impedance low-noise cathode follower and preamplifier; input impedance $1{\cdot}2 \times 10^8\ \Omega$; approximate gain 50.

The voltage developed at the pressure transducer was detected by a high-impedance cathode follower and a low-noise amplifier with a maximum gain of 10^5. Figure 2 is a circuit diagram for the input stage of the amplifier. The input impedance of the cathode follower is $1{\cdot}2 \times 10^8\ \Omega$, and the gain of the pre-amplifier is approximately 50. The root-mean-square noise level referred to the input with the transducer connected to the cathode follower is approximately $5\ \mu$V for a frequency band from 20 to 20,000 c/s. The bulk of the noise occurs at low frequencies and can be attributed to fluctuations in the cathode-follower grid current, which develops quite large voltage fluctuations across the capacitive impedance of the lead-zirconate pressure transducer. To reduce the fluctuations in grid current, dirt and moisture must be kept from the input circuitry and transducer. When the transducers were not being used and the air humidity was

high, it was necessary to store the input circuitry and transducer in an air-tight box containing a drying agent.

The electrical signals from the pressure transducers were recorded on separate channels of a magnetic tape using an Ampex FR 1100 tape recorder. The tape recorder was fitted with a specially designed playback-head assembly that allowed one signal to be time-delayed with respect to the other. The correlation of pressure signals was measured by a thermocouple that was first fed with the sum and then with the difference of the time-delayed signals from the tape recorder. The thermocouple response was detected by a model SEW 5 millivoltmeter manufactured by the Sensitive Research Corporation. The correlation between two signals was obtained by subtracting the thermocouple response to the difference between two signals from the response to the sum of the signals. Provisions were made to allow the sum and difference signals to be filtered by a Krohn-Hite model 310-AB variable band-pass filter just before they entered the thermocouple.

Measurements of the spectrum of the pressure were made by passing the signal through a General Ratio type 736-A wave analyser whose output was fed to the thermocouple. Root-mean-square measurements were made with a Ballantine model 320 true RMS meter. Electrical signals were monitored with a DuMont model 322-A dual-beam oscilloscope.

2.2. *Co-ordinate system and nomenclature*

A Cartesian co-ordinate system is chosen to describe the measurements. The x- and z-axes lie in the plane of the wall with x increasing in the stream direction. The y-axis is normal to the wall.

Other notations used in the description of the measurements include: ρ the air density; δ the boundary-layer thickness; q the dynamic pressure of the mean flow; R the Reynolds number based on the distance from the virtual origin of the turbulent boundary layer; τ_w the wall shear stress; $U_\tau = (\tau_w/\rho)^{\frac{1}{2}}$ the friction velocity; U the mean velocity in the stream direction; $\Delta U/U_\tau$ the displacement of the boundary-layer mean-velocity profile produced by surface roughness; and τ a time delay. The subscript ∞ refers to free-stream conditions.

3. Experimental environment

The accuracy or validity of the experiments can be affected by the vibration of the pressure transducer, the sound field and turbulence in the flow, and the state of the turbulent boundary layer. The various factors affecting the experimental environment will be discussed separately. The discussion refers, unless otherwise stated, to the highest available wind-tunnel speed, 200 ft./sec, because disturbing factors were largest at high speeds.

3.1. *Vibration of the pressure transducer*

Very effective vibration isolation of the pressure transducers was obtained with the sand-filled tubular-steel mounting described in § 2. The effectiveness of the mounting was tested by shielding the transducer from the wall-pressure fluctua-

tions while the tunnel was running. It was found that the signals caused by vibration amounted to less than $\frac{1}{100}$ of the mean-square turbulent wall-pressure fluctuations.

3.2. *Sound field in the test section*

Before the wall-pressure measurements were made, the sound-pressure level and spectrum of the sound field in the settling chamber were measured in a frequency band of from 25 to 7500 c/s, with a General Radio sound-level meter and sound analyser. The spectral density of the sound had a peak at 135 c/s, and at higher frequencies was approximately proportional to the inverse square of the frequency. The mean-square sound pressure was $\frac{1}{32}$ of the mean-square wall-pressure fluctuations that were measured later.

The sound-pressure level in the settling chamber may not accurately represent the sound-pressure level in the test section. To measure the test-section sound directly, a pressure transducer was installed flush with the surface and on the stagnation line of a streamlined model shaped like a wing tip that was exposed to the airflow in the test section.

The mean-square stagnation-pressure fluctuations were found to be approximately $\frac{1}{16}$ of the mean-square wall-pressure fluctuations over a frequency band extending from 105 to 20,000 c/s. Examination of the spectra of the stagnation-pressure fluctuations revealed peaks of the energy density at 135 and 200 c/s. The peak at 135 c/s corresponds to the sound produced by the wind-tunnel fan. The peak at 200 c/s was not present in the settling chamber sound. The settling-chamber-sound spectrum was measured about $1\frac{1}{2}$ years before the stagnation-point pressure spectrum, and it is possible that the additional sound may be caused by changes in the structural vibration of the tunnel, test section, or fan section. At frequencies above 200 c/s, the stagnation-point pressure spectrum decreased approximately linearly with frequency. However, the energy density varied from day to day, and even while the spectrum was being measured. We do not believe that the spectral measurements above 200 c/s give a reliable estimate of the sound field in the test section. At times the streamlined model itself would rattle and produce measurable contributions to the spectra above 200 c/s.

A more precise way to estimate the sound field in the test section was discovered later in the investigation. During the measurements of the longitudinal space-time correlation of the wall pressure, it was discovered that a small peak in the correlation occurred for negative time delay. The location of the peak corresponded to the speed of sound in the test section and indicated that sound was propagating upstream from the diffuser. These observations are described more completely in § 5.1. The magnitude of the extraneous signal produced by sound in the test section is finally determined in § 5.1 to be $\frac{1}{20}$ of the wall-pressure fluctuations.

3.3. *Turbulence in the test section*

The wind tunnel does not have a honeycomb, but the settling chamber is fitted with four turbulence-damping screens. The turbulence level in the centre of the test section rises with speed and has been measured at speeds of 50, 100 and

150 ft./sec. By extrapolation to 200 ft./sec, the speed used in the bulk of the present work, the turbulence level of the axial velocity component near the centre of the test section is approximately $(\overline{u'^2})^{\frac{1}{2}}/U_\infty = 6 \times 10^{-4}$. The transverse velocity in the centre of the test section is three times the axial velocity, $(\overline{v'^2})^{\frac{1}{2}}/(\overline{u'^2})^{\frac{1}{2}} = 3$, at all speeds. If one assumes that the sound field in the test section consists of plane waves propagating in one direction, the root-mean-square velocity fluctuations associated with sound would amount to approximately $(\overline{u'^2})^{\frac{1}{2}}/U_\infty = 10^{-4}$. It seems certain that the majority of the turbulent velocity fluctuations in the test section are produced by vorticity or entropy fluctuations.

Additional information about the turbulence in the wind tunnel near the wall was obtained from the initial wall-pressure measurements beneath the turbulent boundary layer (see § 4). After the tunnel was started and the wind-tunnel air had reached an equilibrium velocity, the mean-square wall-pressure fluctuations from 5 to approximately 100 c/s were very great, but slowly decreased monotonically with time, and 30 min later reached an equilibrium value that was an order of magnitude lower than the initial value. Examination of the spectrum of these wall-pressure fluctuations showed that the energy density was greatest at low frequencies. It was also noticed that the mean-square and low-frequency spectrum of the wall-pressure fluctuations did not decrease after starting the tunnel if the sun was shining. If the tunnel was run at night or on a cloudy day, the mean-square and low-frequency spectrum of the wall pressure would reach low values. On a few occasions, the mean-square wall pressure was observed to decrease as the sun was obscured by clouds and increase again when the sun reappeared.

The streamlines near the wall in the contraction section were observed using the dense white smoke produced when titanium tetrachloride is exposed to air. Large-scale oscillations of the streamlines near the wall were observed above the concave surface of the contraction section. The large-scale eddies produced in the contraction section were carried into or just above the test-section boundary layer. We believe that low-frequency large-scale flow disturbances are produced by the combined effects of Taylor–Goertler boundary-layer instability and density stratification of the air near the wind-tunnel wall. Density stratification is produced by heat transfer through the steel shell of the wind tunnel. When the density-stratified air is accelerated into the test section, vorticity is produced and causes the large-scale, low-frequency wall-pressure fluctuations.

Examination of many wall-pressure spectra showed that above approximately 100 c/s the spectra are always repeatable and independent of the temperature of the wind-tunnel shell.

3.4. *The nature of the turbulent boundary layer used in the investigation*

The turbulent boundary layer developed on the lower surface of the test section was used in the investigation. Figure 1 shows the dimensions of the lower surface of the wind-tunnel contraction and test section. The lower surface of the test section was covered with sheets of varnished masonite to provide a smooth surface for the development of the boundary layer. The majority of the measure-

ments were made at a speed of 200 ft./sec, and all with natural transition of the boundary layer.

To allow the results of this investigation to be repeated or compared with other experiments, the properties of the turbulent boundary layer in the test section must be investigated and compared with an accepted standard for the equilibrium turbulent boundary layer. The ideal turbulent boundary layer defined by Coles (1953) was selected as the standard.

Boundary layer	U_∞ ft./sec	R_θ	δ	δ^*	θ	δ^*/θ	U_τ/U_∞	R
Actual	204	38,000	0·42	0·041	0·0315	1·3	0·0326	$3{\cdot}1 \times 10^7$†
Ideal	—	38,000	—	—	—	1·3	0·0318	$3{\cdot}2 \times 10^7$
Actual	156	29,000	0·374	0·038	0·034	1·25	0·0331	$2{\cdot}5 \times 10^7$†
Ideal	—	29,000	—	—	—	1·31	0·0325	$2{\cdot}3 \times 10^7$

† Assumed origin of boundary layer at station 10 of figure 1.

TABLE 1. Properties of the actual and ideal turbulent boundary layer.

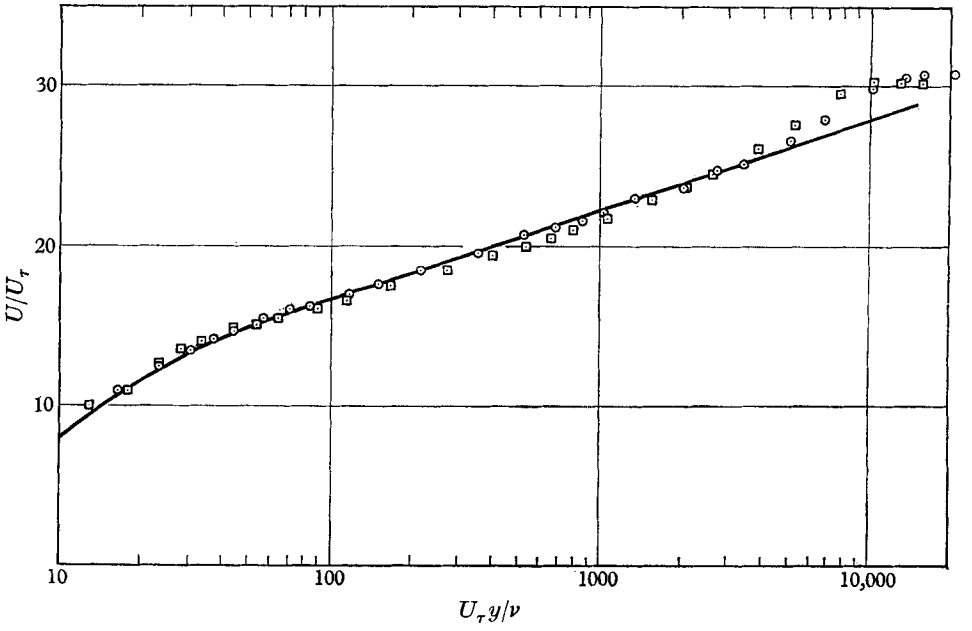

FIGURE 3. Mean-velocity profiles in the turbulent boundary layer with natural transition. Refer to table 1 for other parameters describing the boundary layer. —, Coles' ideal turbulent boundary layer. ⊙, $R_\theta = 38{,}000$, $U_\infty = 204$ ft./sec; ⊡, $R_\theta = 29{,}000$, $U_\infty = 156$ ft./sec.

The properties of the turbulent boundary layer were measured with a Stanton tube and a Pitot tube. The shearing stress at the wall was obtained from the Stanton-tube measurements by use of the data and results of Stanton-tube calibration presented by Bradshaw & Gregory (1961). From the Pitot-tube measurements the mean-velocity profile, boundary-layer thickness, displacement thickness, and momentum thickness were obtained.

These measured properties of the boundary layer are tabulated and compared in table 1 with the properties that the ideal boundary layer would have if the Reynolds number R_θ based on momentum thickness were the same. The velocity profiles have been plotted in figure 3, where the velocity profile of the ideal boundary layer is also shown. Examination of table 1 and figure 3 shows that the properties of the boundary layer at 204 ft./sec agree reasonably well with the properties of the ideal boundary layer. At 150 ft./sec, the value of the measured shape parameter, i.e. displacement thickness δ^* divided by momentum thickness θ, is considerably lower than the value of the ideal shape parameter, and some deviation from the ideal velocity profile is also apparent in figure 3. Apparently, the boundary layer with natural transition has not completely reached an equilibrium state at the speed 150 ft./sec. The turbulent boundary layer produced by natural transition at 200 ft./sec was judged to represent a reasonable approximation to the ideal turbulent boundary layer, and was used for the majority of the wall-pressure measurements. A few measurements of mean-square wall-pressure fluctuations were made beneath boundary layers that were tripped or developed on a rough surface. The properties of these boundary layers are discussed along with the measurements of the fluctuating wall pressure beneath them in § 4.2.

4. Root-mean-square and power spectrum of the wall pressure

The wall pressure is a stationary random function of time t and position coordinates x, z. We use the theory of stationary random functions to interpret the pressure fluctuations that are measured. The quantities measured are the correlation or covariance of the pressure p, i.e.

$$R_{pp}(x_1, x_3, \tau) = \frac{\overline{p(x, z, t)\, p(x+x_1, z+x_3, t+\tau)}}{\sqrt{\{\overline{p^2(x, z, t)}\, \overline{p^2(x+x_1, z+x_3, t+\tau)}\}}}, \tag{1}$$

and the temporal Fourier transform of the autocorrelation of the pressure defined by

$$\overline{p^2} R_{pp}(0, 0, \tau) = \int_0^\infty E(\omega) \cos \omega\tau \, d\omega, \tag{2}$$

where

$$E(\omega) = (\pi)^{-1} \int_0^\infty \overline{p^2} R_{pp}(0, 0, \tau) \cos \omega\tau \, d\tau \tag{3}$$

is the power spectrum of the pressure.

When the first measurements of the wall pressure were made, it was found that the power spectrum of the pressure fluctuations contained a large energy density at low frequencies, which varied from day to night and also when the amount of sunlight shining on the tunnel changed during the day. For example, we have obtained spectra measured on the same day with different amounts of sunlight and have found differences between the spectra amounting to a factor of ten or more at frequencies below $\omega\delta^*/U_\infty = 0{\cdot}05$ ($f = 40$c/s). The variation in the pressure spectrum at low frequencies is attributed to density stratification of the air near the wind-tunnel wall as already discussed in § 3.3. The spectra of the wall pressure above a dimensionless frequency $\omega\delta^*/U_\infty = 0{\cdot}14$ were always

repeatable and scaled with the wind-tunnel speed and boundary-layer-displacement thickness. Therefore the present experiments were restricted to frequencies produced by the fluctuating pressures in the boundary layer above $\omega\delta^*/U_\infty = 0{\cdot}14$.

In the measurements of the mean-square pressure and space-time correlation of the pressure, we used the Krohn–Hite filter to reject all frequencies below $\omega\delta^*/U_\infty = 0{\cdot}14$. For the boundary layer developed at 200 ft./sec, with displacement thickness $\delta^* = 0{\cdot}041$ ft., and thickness $\delta = 0{\cdot}42$ ft., the wavelength associated with a convected eddy that produces pressure fluctuations at $\omega\delta^*/U_\infty = 0{\cdot}14$ is $3{\cdot}9\delta$. Thus we can certainly obtain information about eddies whose scale is of the order of one or two boundary-layer thicknesses even when we reject signals below $\omega\delta^*/U_\infty = 0{\cdot}14$.

4.1. *Boundary layers developed on a smooth surface with natural transition*

The power spectra of the wall-pressure fluctuations measured at 150 and 200 ft./sec, with natural transition on a smooth surface, are shown in figure 4. The vertical dashed line shows the dimensionless frequency $\omega\delta^*/U_\infty = 0{\cdot}14$ below which the spectra were not always repeatable. The dimensionless spectra of figure 4 at 150 ft./sec agree very well with the spectra obtained at 200 ft./sec, even though the boundary-layer shape parameter at 150 ft./sec does not agree with the ideal boundary-layer shape parameter.

The root-mean-square wall pressure was measured on ten different occasions at 200 ft./sec, and on five different occasions at 150 ft./sec, over a frequency band $0{\cdot}14 < \omega\delta^*/U_\infty < 28$. The average of the wall-pressure measurements was corrected for the effect of extraneous signals from the transducer. From the tests of sound, vibration and turbulence in the wind tunnel, we estimate that approximately $\frac{1}{20}$ of the measured mean-square-wall pressure fluctuations were produced by extraneous signals which were uncorrelated with the turbulent pressure fluctuations in the boundary layer. The extraneous signals were caused primarily by upstream propagating sound in the test section, as explained in §§ 3.2 and 5.1.

The corrected value of the root-mean-square wall pressure is $(\overline{p^2})^{\frac{1}{2}}/\tau_w = 2{\cdot}19$ at 200 ft./sec, and $(p^2)^{\frac{1}{2}}/\tau_w = 2{\cdot}15$ at 150 ft./sec.

4.2. *Increase in the root-mean-square wall pressure and power spectrum caused by surface roughness and a boundary-layer trip*

The value of the root-mean-square wall pressure reported in the previous section was exceeded when the boundary layer was tripped or developed on a rough surface.

The surface roughness was produced by machine-tool marks on the unlapped surface of the 20 in. diameter steel disk in which the transducers were mounted, and by slight misalignment ($\pm$ 0·004 in.) of the dummy transducers in their holes upstream of the transducer. Elsewhere, the wall was smooth and in the same condition as it was for the measurements of § 4.1. The wall-pressure measurements and the properties of the boundary layer are shown in table 2. The quantity $\Delta U/U_\tau$ is the amount that the logarithmic portion of the mean velocity profile of the boundary layer was displaced from the equilibrium velocity profile of

figure 3 when the surface was rough. The change in the boundary-layer turbulence caused by the roughness results in an increase in fluctuating wall pressure and wall shear. However, the increase in wall shear is not as great as the increase in

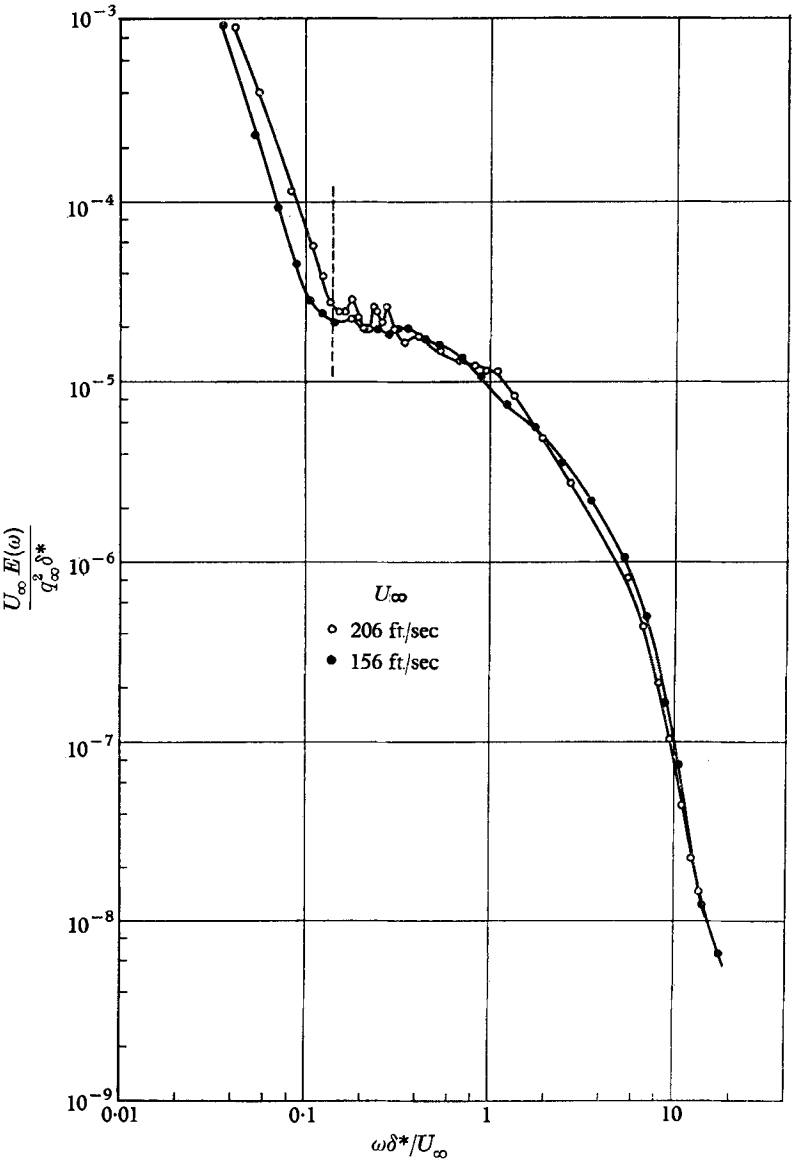

FIGURE 4. Dimensionless power spectrum of the wall pressure. Vertical dashed line shows the frequency below which signals were rejected in the subsequent measurements.

the fluctuating wall pressure (see table 2). The power spectrum of the wall-pressure fluctuations on the rough surface was also measured, and was increased, at all frequencies, by the ratio of the mean-square pressures measured on rough and smooth surfaces. The pressure-fluctuation measurements on the rough steel

disk demonstrate that surface roughness on even a small portion of the wall can have a profound effect on the fluctuating wall pressure in the immediate vicinity.

We can illustrate the effect of surface roughness extended over the whole wall, and of disturbances in the boundary layer caused by a trip, from the results of tests made at the beginning of this investigation. A two-dimensional boundary-layer trip (a square $\frac{1}{2} \times \frac{1}{2}$ in. strip of wood) was placed on the wall 9 ft. ahead of the transducer. In this case the wall was already rough everywhere (rough, unfinished plywood), and the steel plate was rough as described above. The

$(\overline{p^2})^{\frac{1}{2}}/q_\infty \times 10^3$	$(\overline{p^2})^{\frac{1}{2}}/\tau_w$	U_∞	U_∞/U_τ	$\Delta U/U_\tau$	Condition
4·66	2·19	204	30·7	0	Smooth plate
7·0	3·09	205	29·7	−2·36	Rough plate
4·7	2·15	156	30·1	0	Smooth plate
6·6	2·63	153	28·2	−2·36	Rough plate

TABLE 2. Effect of wall roughness on wall-pressure fluctuations.

$(p^2)^{\frac{1}{2}}/\tau_w$	$(p^2)^{\frac{1}{2}}/q_\infty \times 10^3$	Re_θ	Source	Remarks
3·24	9·5	3,800	Harrison (1958)	Extraneous noise not known
2·32	5·5	13,000	Willmarth (1959)	Transducer too large. $d/\delta^* = 1{\cdot}1$
2·49	5·7	22,600	—	Boundary layer tripped
0·97	1·9	65,000	Skudrzyk & Haddle (1960)	Measured in water. Large transducer, $d/\delta^* = 2{\cdot}5$
3·5	Unknown	Unknown	Kistler	Reported by Laufer (1961)
2·15	4·7	29,000	Present	Relatively small transducer,
2·19	4·66	38,000	Investigation	$d/\delta^* = 0{\cdot}33$
2·5	Not applicable		Corcos (1962)	$Re_d = 6 \times 10^4$ } Turbulent flow
2·0	—		—	$Re_d = 2 \times 10^5$ } in a tube

TABLE 3. Summary of some results of wall-pressure measurements beneath turbulent boundary layers.

root-mean-square wall pressure before the trip was in place was $(\overline{p^2})^{\frac{1}{2}}/q_\infty = 0{\cdot}008$, but this was increased to 0·0097 when the trip was in place. In this case also, the power spectrum with the trip and a rough wall was almost the same as the power spectrum shown in figure 4, if the power spectrum of figure 4 at each frequency is multiplied by the ratio of the appropriate mean-square pressures. Unfortunately, we are unable to relate the root-mean-square wall pressure to the wall shear stress because the mean velocity profile was not correctly measured in these tests with the trip and with roughness everywhere on the wall.

4.3. *Root-mean-square wall-pressure measurements of this and other investigations*

Any comparison of measurements of the root-mean-quare wall pressure must be interpreted in the light of the effects that Reynolds number, surface roughness, and other disturbances can have on the fluctuating pressure. Table 3 shows the results of this and a number of other investigations of fluctuating wall pressures.

We do not know enough about the experimental environment in most of the other investigations to decide why different values of $(\overline{p^2})^{\frac{1}{2}}/\tau_w$ were observed. The results of Corcos (1962) show quite clearly that in a tube the ratio $(\overline{p^2})^{\frac{1}{2}}/\tau_w$ slowly decreases as the Reynolds number increases. Reliable measurements in a boundary layer with systematic variation of the Reynolds number have not yet been reported.

5. Longitudinal space-time correlation of the wall pressure

5.1. *The measurements of the longitudinal space-time correlation of the wall pressure*

The correlation $R_{pp}(x_1, 0, \tau)$ of the wall pressure measured at two points, one directly downstream of the other but separated by a distance x_1 in the stream direction was investigated at a free-stream speed of 200 ft./sec. The pressure signals from the two transducers were recorded simultaneously on magnetic tape and were played back with a variable time delay between one signal and the other. The correlation $R_{pp}(x_1, 0, \tau)$ between the time-delayed pressure signals for various spatial separation x_1 and time delays τ are shown in figure 5. In this figure the origin $\tau = 0$ (indicated by a short vertical line) has been shifted to the left to display the maxima of the wall-pressure correlations beneath each other. The pressure-fluctuation signals were filtered so that only frequencies from $105 < f < 10{,}000$ c/s (i.e. $0{\cdot}14 < \omega\delta^*/U_\infty < 13{\cdot}6$) are included in the measurements.

Some remarks about the effect of the filter on the pressure correlation are necessary. First, the value of $R_{pp}(x_1, 0, \tau)$ is not changed appreciably by the high-frequency cut-off at 10,000 c/s where the power spectral density is small (see figure 4). The lower-frequency cut-off at 105 c/s produces the major effect. The magnitude of this effect can only be estimated because the true power spectrum of the pressure is masked by the low-frequency pressure fluctuations produced by large-scale density stratification in the boundary layer.

If we assume that the power spectrum of the pressure below 105 c/s is constant and equal to the value at 105 c/s, the measured value of the autocorrelation of the pressure $R_{pp}(0, 0, \tau)$ of figure 5 can be corrected using equation (2). The corrected value of $R_{pp}(0, 0, \tau)$ has been computed and is shown in figure 11, where it is presented as a spatial correlation in a moving reference frame with $\tau = x_1/U_c$. The corrected value of $R_{pp}(0, 0, \tau)$ is unchanged at $\tau = 0$, does not oscillate, and is greater than the measured autocorrelation for all τ. The greatest correction to the measured autocorrelation occurs over the range $2 < \tau U_\infty/\delta^* < 16$ and causes an increase of 14 % at most.

If it is assumed that the power spectrum of the pressure below 105 c/s falls linearly to zero at $\omega = 0$, the corrected autocorrelation is at most 6 % greater than the measured autocorrelation of figure 5. The corrected autocorrelation will now oscillate because $E(\omega) = 0$ [see equation (3)]. The first and only zero crossing of the autocorrelation of the pressure occurs at $\tau U_\infty/\delta^* = 5$ instead of 3.

We must conclude that the nature of the spectral density of the pressure below 105 c/s will control the behaviour of the tail of the pressure correlation; however,

the maxima of the pressure correlation are not appreciably affected by the filter. The correlation measurements of figure 5 show that the wall-pressure fluctuations appear to be convected downstream ($\tau > 0$) at a fraction greater than half the stream speed. A small portion of the wall-pressure fluctuations appear to be moving upstream ($\tau < 0$) at a much higher speed, approximately 1200 ft./sec. The upstream propagation of pressure fluctuations is undoubtedly caused by

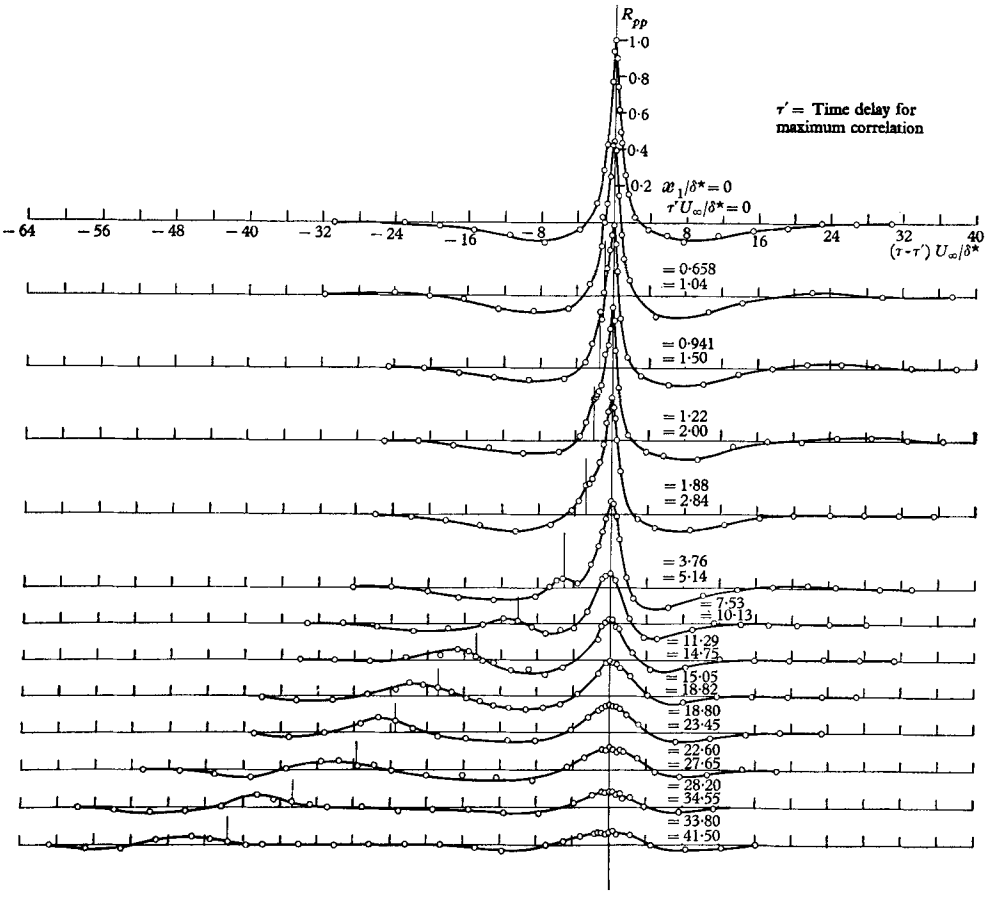

FIGURE 5. Measured values of the longitudinal space-time correlation of the wall pressure. The displaced origins, $\tau = 0$, are indicated by a short vertical line. τ' = time delay for maximum correlation.

sound waves produced in the wind-tunnel diffuser and fan, which travel upstream through the test section towards the settling chamber. We have determined the frequency of the upstream propagating sound field by filtering out pressure signals at low frequencies, and measuring the correlation $R_{pp}(x_1, 0, \tau)$ over the restricted frequency range $300 < f < 10{,}000$ c/s (i.e. $0{\cdot}41 < \omega\delta^*/U_\infty < 13{\cdot}6$). In this case there was no longer any correlation between the wall pressures when τ is less than zero and x_1 is large. Therefore, the majority of the sound pressure is produced by sound waves with a frequency below 300 c/s. The measurements of the power spectrum of the wall pressure, figure 4, at 206 ft./sec, show small

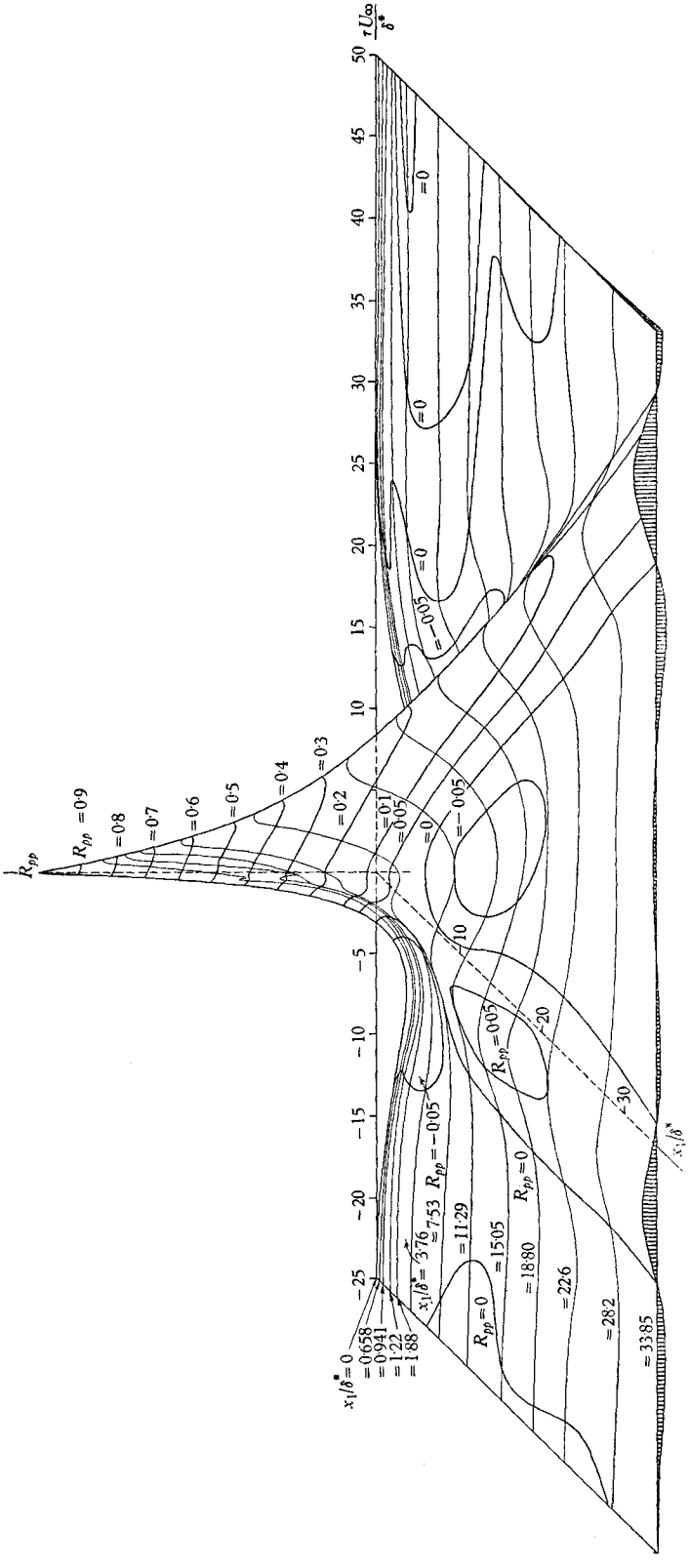

FIGURE 6. Longitudinal space-time correlation of the wall pressure displayed in three dimensions using the data of figure 5.

peaks apparently caused by the upstream propagating sound in the frequency band $105 < f < 300$ c/s (i.e. $0{\cdot}14 < \omega\delta^*/U_\infty < 0{\cdot}41$). The mean-square sound pressure in the test section can be estimated from the average maximum value of $R_{pp}(x_1, 0, \tau)$ for $\tau < 0$ (approximately $R_{pp}(x_1, 0, \tau) = 0{\cdot}05$). This value is approximately the ratio of mean-square sound pressure in the test section to mean-square pressure measured by the transducer. We have used this value in § 4.1 to estimate the true value of the root-mean-square wall pressure.

To display the correlation measurements in terms of non-dimensional spacing x_1/δ^* and time delay, $\tau U_\infty/\delta^*$, a three -dimensional drawing, figure 6, of the wall-pressure correlation has been constructed from the data of figure 5.

5.2. *Convection speed of large- and small-scale pressure producing eddies*

The measured correlations displayed in figure 6 suggest that, in a frame of reference moving in the stream direction, $x_1 > 0$, $\tau > 0$, the time variation of the wall pressure would be reduced. One can define an integral time scale and by quadratures determine the (constant) velocity of a frame of reference in which the time scale is the greatest (Phillips 1957). We shall not define an integral time scale but will consider instead the trajectory in space and time of a reference frame in which the decay of the pressure correlation at each time delay is the least. This trajectory will correspond to the average trajectory of an observer who follows the pressure-producing eddy systems as they move downstream and decay. The trajectory, in the (x_1, τ)-plane, of the reference frame in which the decay of R_{pp} is the least is the locus of points on the lines $R_{pp} = \text{const.}$ which have the greatest values of τ. This trajectory is shown as a heavy solid line on the contour map of the pressure correlation, figure 7, which was obtained from the data of figure 5. The slope $dx_1/d\tau$ of the trajectory shown in figure 7 may be considered to be the speed of the reference frame in which the rate of decay of a given pattern of wall pressure is the least. When x_1 or τ are small, the speed of the reference frame is less than it is for larger spacings x_1 or later times τ. The increase in speed of the reference frame is caused by the decay of small pressure-producing eddies near the wall where the mean speed is low. When the smaller eddies have decayed, the observer interested in a certain initial pressure configuration must move faster to keep up with the more rapidly moving large-scale remnants of the original pressure pattern. Eventually (x_1 and τ large), nothing of the original configuration remains and $R_{pp} = 0$. The speed of the reference frame in which the rate of decay of the pressure correlation is the least will be called the convection speed of the pressure-producing eddies, and will be considered to be a function of x_1/δ^*. Figure 8 shows the convection speed obtained from the slope of the heavy line in figure 7. The convection speed varies from $U_c/U_\infty = 0{\cdot}56$ when $x_1/\delta^* = 0$ to an asymptotic value $U_c/U_\infty = 0{\cdot}83$ for large x_1/δ^*. The asymptotic value of the convection speed might be somewhat greater if low-frequency pressure fluctuations produced by large eddies had not been rejected by the filter. (Wavelengths greater than $3{\cdot}9\delta$ have been rejected.)

The pressure correlations in frequency bands centred at low and at high frequencies have been investigated. The correlation in a frequency band was measured by passing the sum and then the difference of the two pressure signals

through the band-pass filter before the sum and difference signals were squared and averaged by the thermocouple. The passage of any pair of correlated random signals through a band-pass filter will produce oscillations of the correlation between the signals. A classical example is the diffraction of light by a slit. It

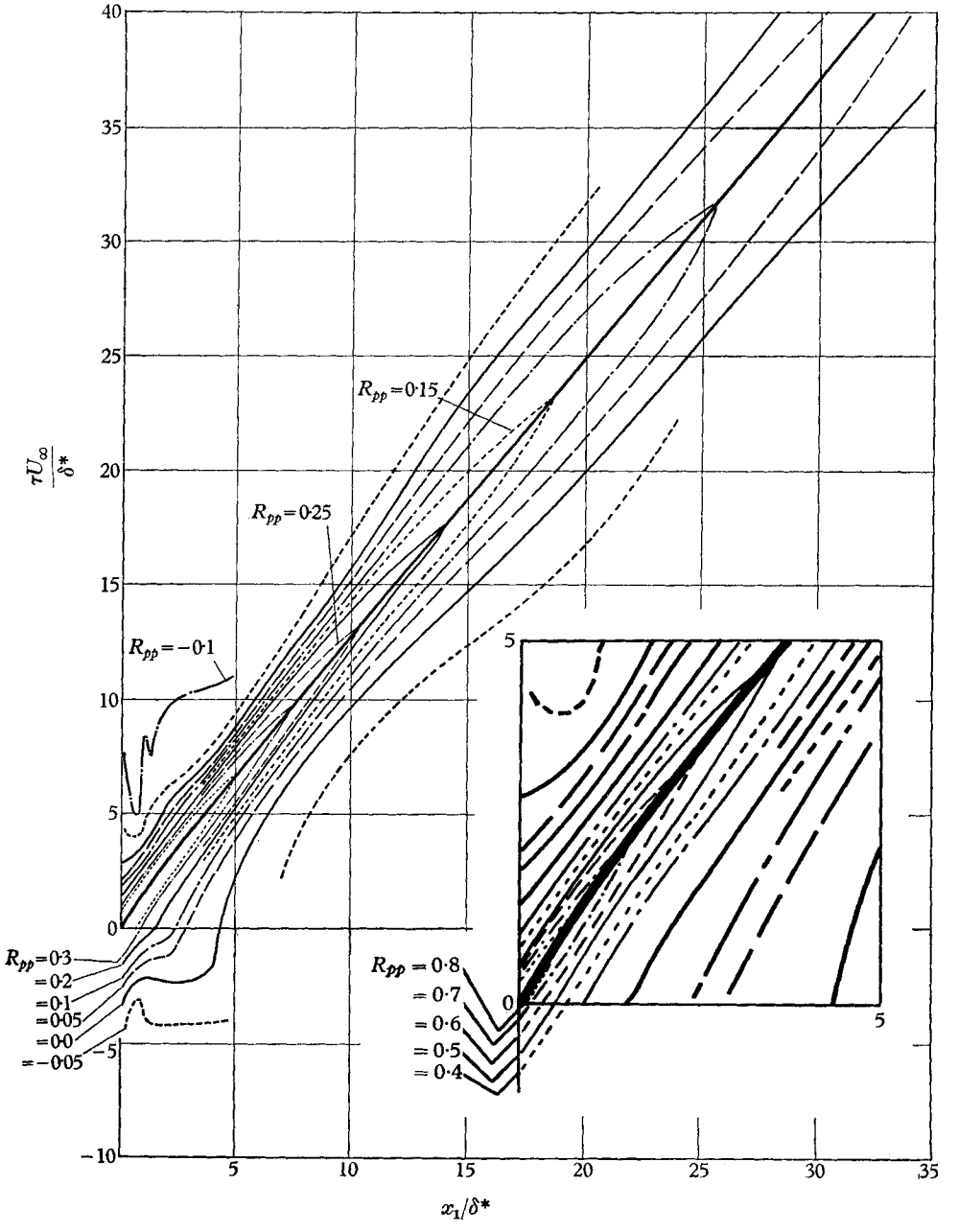

FIGURE 7. Contour map of the longitudinal space-time correlation data of figure 5. The heavy line represents the trajectory of a reference frame in which the rate of decay of the pressure correlation is the least.

may be unnecessary to remark that in general the structure of the correlation between two signals passed through a narrow-band filter is more dependent on the characteristics of the filter than on the characteristics of the original signal. We must not attach any deep significance to oscillations of the pressure correlation produced by the filter.

The pressure correlation in two frequency bands, $300 < f < 700$ c/s and $3000 < f < 5000$ c/s, was measured as a function of x_1 and τ. Most of the sound in the test section is below 300 c/s and cannot affect these measurements. The pressure correlation in each frequency band was normalized by dividing by the

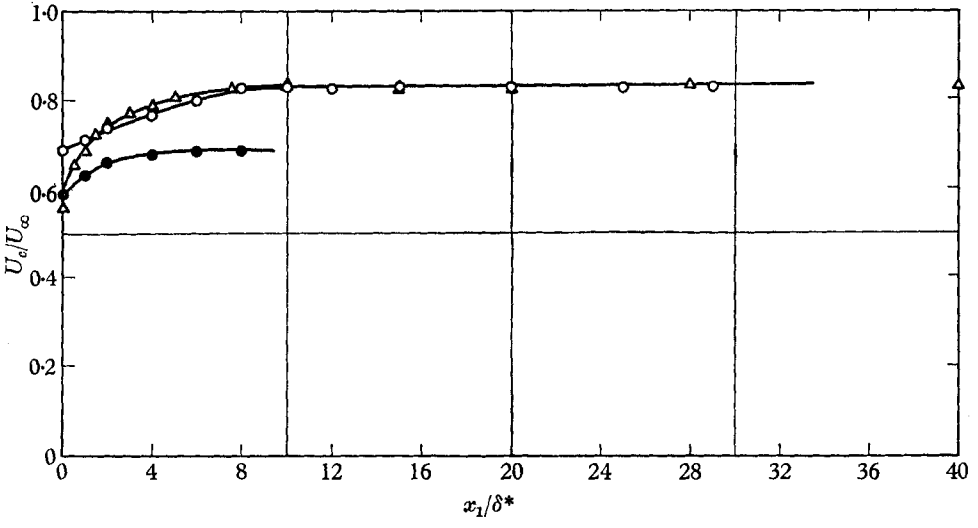

FIGURE 8. Local convection speed of pressure-producing eddies for various frequency bands. ○, $300 < f < 700$, $0{\cdot}41 < \omega\delta^*/U_\infty < 0{\cdot}95$; ●, $3000 < f < 5000$, $4{\cdot}1 < \omega\delta^*/U_\infty < 6{\cdot}8$; △, $105 < f < 10{,}000$, $0{\cdot}14 < \omega\delta^*/U_\infty < 13{\cdot}6$.

autocorrelation of the pressure, $R_{pp}(0, 0, \tau)$, in that frequency band. For any particular spacing $x_1 > 0$ between the transducers, the correlation function in a given frequency band is an oscillating function of τ. As τ is increased, the correlation function oscillates with increasing amplitude until a maximum amplitude is reached and then oscillates with decreasing amplitude until it vanishes. Figure 9 shows only the peak of maximum amplitude of the correlation function for each transducer spacing x_1. Numerous experimentally measured points have not been shown on this plot. In general the scatter was quite small, generally less than 5 %.

An approximate convection speed of large and small eddies may be obtained from the values of x_1 and τ where the correlation peaks are tangent to their envelope. Figure 8 shows the speed of a reference frame (convection speed) moving with the eddies that produce low- and high-frequency pressure fluctuations. Convection speed in either frequency band is lower when x_1 is small and rises as x_1 increases, presumably because the chosen frequency bands were not narrow enough to isolate completely a single eddy size. However, all the convection speeds in the

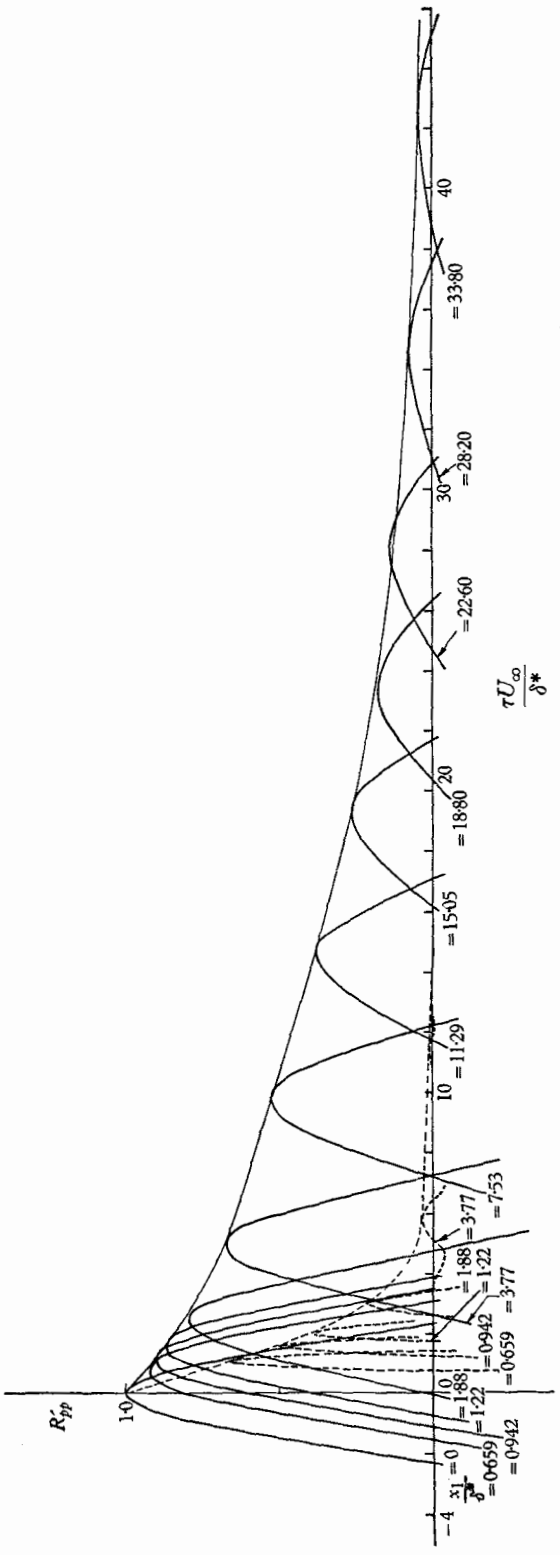

FIGURE 9. Peaks of the longitudinal space-time correlation in a low- and a high-frequency band. See equation (9).
——, $300 < f < 700$, $0{\cdot}41 < \omega\delta^*/U_\infty < 0{\cdot}95$; - - - -, $3000 < f < 5000$, $4{\cdot}1 < \omega\delta^*/U_\infty < 6{\cdot}8$.

high-frequency band are lower than those in the low-frequency band. The asymptotic value of the convection speed is $U_c/U_\infty = 0{\cdot}69$ in the frequency band of from 3000 to 5000 c/s (i.e. $4{\cdot}1 < \omega\delta^*/U_\infty < 6{\cdot}8$), and $U_c/U_\infty = 0{\cdot}83$ in the frequency band of from 300 to 700 c/s (i.e. $0{\cdot}41 < \omega\delta^*/U_\infty < 0{\cdot}95$). These different convection speeds show that large pressure-producing eddies move faster on the average than smaller eddies (assuming that low- and high-frequency pressure fluctuations are caused by large and small eddies, respectively).

5.3. *Decay of large- and small-scale pressure-producing eddies*

The envelopes of the peaks of maximum pressure correlation in low- and high-frequency bands (see figure 9) show that the pressure correlation in a high-frequency band decays more rapidly (with increasing x_1) than the correlation in a low-frequency band. We can put this observation on a more definite basis by considering the pressure correlation and spectra in a moving reference frame.

Consider the temporal Fourier transform $F(x_1, 0, \omega)$ of the pressure correlation $R_{pp}(x_1, 0, \tau)$ defined by

$$R_{pp}(x_1, 0, \tau) = \int_{-\infty}^{\infty} F(x_1, 0, \omega)\, e^{i\omega\tau}\, d\omega. \tag{4}$$

Let us define a co-ordinate system (x', y', z') whose origin moves downstream at the convection speed of the eddies which produce the pressure fluctuations, x' being positive in the upstream direction. The spatial separation of the pressure transducers in the fixed and moving systems is related to the time delay between signals from the transducers by

$$\tau = \frac{x_1 + x_1'}{U_c}, \tag{5}$$

where x_1 and x_1' are the spatial separations in the fixed and moving systems, respectively. If we assume that the pressure fluctuations are produced by a convected pattern of eddies which changes slowly with time, the frequency of signals observed in the stationary frame is related to the wave-number of the convected pressure pattern by $\omega = U_c k$. Under this transformation, equation (4) becomes the spatial correlation of the pressure in a moving reference frame.

$$R_{pp}\left(x_1, 0, \frac{x_1 + x_1'}{U_c}\right) = \int_{-\infty}^{\infty} U_c F(x_1, 0, U_c k)\, e^{ikx_1}\, e^{ikx_1'}\, dk. \tag{6}$$

The spatial spectrum function in the moving frame (the inverse of equation (6)), i.e.

$$U_c F(x_1, 0, U_c k)\, e^{ikx_1} = \int_{-\infty}^{\infty} R_{pp}\left(x_1, 0, \frac{x_1 + x_1'}{U_c}\right) e^{-ikx_1'}\, dx_1', \tag{7}$$

should not depend on x_1 if the pressure pattern does not change as it is connected downstream. Actually, the spectral function in the moving frame will decay as x_1 increases.

It is possible to measure experimentally the decay of the spectral function in the moving reference frame by evaluating the pressure correlation in the stationary reference frame in a narrow frequency band. Consider the pressure

correlation (6) in the moving reference frame evaluated in a narrow wave-number band, $k_1 < k < k_2$, at the origin $x_1' = 0$ of the moving reference frame:

$$R_{pp}\left(x_1, 0, \frac{x_1+0}{U_c}\right) = 2\int_{k_1}^{k_2} Re\{U_c F(x_1, 0, U_c k)\, e^{ikx_1}\}\, dk. \tag{8}$$

If the wave-number band is small enough, the spectral function (7) in the moving reference frame is approximately constant with respect to k. To examine the

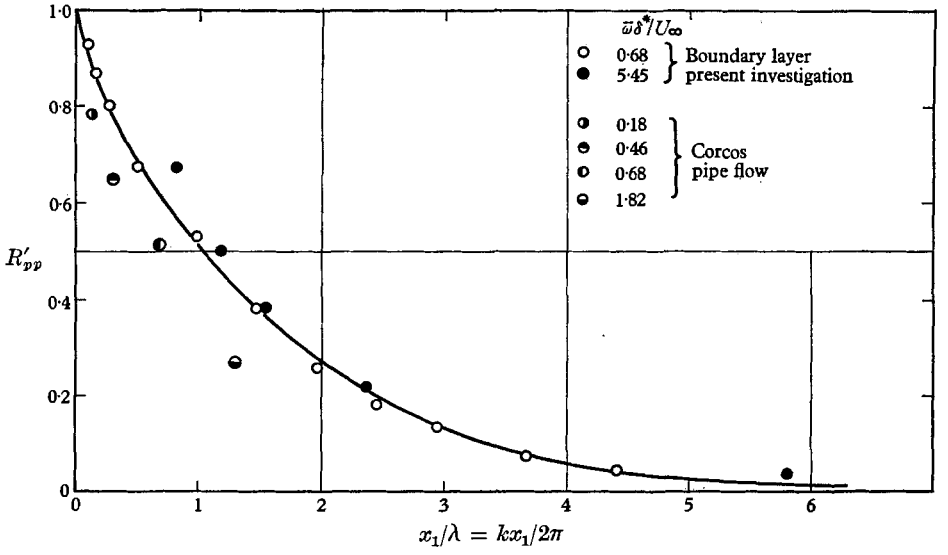

FIGURE 10. Decay of large and small wave-number components of the wall pressure as measured by an observer moving at the eddy convection speed.

decay of the spectral function, we form the ratio of the spectral function at x_1 to the spectral function at $x_1 = 0$, in a narrow wave-number band. The ratio is

$$R'_{pp}\left(x_1, 0, \frac{x_1}{U_c}\right) = \frac{Re\{F(x_1, 0, U_c\bar{k})\, e^{i\bar{k}x_1}\}\,\Delta k}{Re\{F(0, 0, U_c\bar{k})\}\,\Delta k}, \tag{9}$$

where $\bar{k} = \frac{1}{2}(k_2 + k_1)$ and $\Delta k = k_2 - k_1$. This ratio can be obtained experimentally from the maximum value of the pressure correlation in a narrow frequency band divided by the autocorrelation in the band. The peak or maximum values of the normalized pressure correlation measured in a narrow frequency band are displayed in figure 9. It is necessary only to re-interpret ω, $\Delta\omega$, and x_1. If we set

$$\bar{k} = \frac{\bar{\omega}}{U_c} = \frac{\omega_2+\omega_1}{2U_c}, \quad \Delta k = \frac{\Delta\omega}{U_c} = \frac{\omega_2-\omega_1}{U_c} \tag{10}$$

for each peak value of the normalized pressure correlation of figure 9, we obtain the expression R'_{pp} of equation (9). The peak values of the normalized pressure correlation of figure 9 have been plotted in figure 10.

Figure 10 therefore shows the decay of the spectral function R'_{pp} in the moving reference frame for two wave-number bands. We have chosen the asymptotic convection velocity $U_c/U_\infty = 0{\cdot}83$ for the low wave-number band, and $U_c/U_\infty = 0{\cdot}69$ for the high wave-number band. The data plotted in figure 10

show that a given wave-number component, which is inversely proportional to wavelength, of the pressure pattern is destroyed after travelling a distance of approximately four to six wavelengths. Harrison (1958) was the first to report measurements of the spectral function in a narrow wave-number band. He considered frequencies below 2000 c/s and found that the special function had decayed after travelling two wavelengths downstream. We are not able to explain the difference between our results and those of Harrison.

Corcos (1962) has also measured the decay of the spectral function in a fully developed turbulent pipe flow. His results are shown in figure 10. The spectral function R'_{pp} decays more rapidly in turbulent pipe flow than it does in the turbulent boundary layer and is probably a consequence of the greater influence of the solid boundary on the turbulence developed in a pipe.

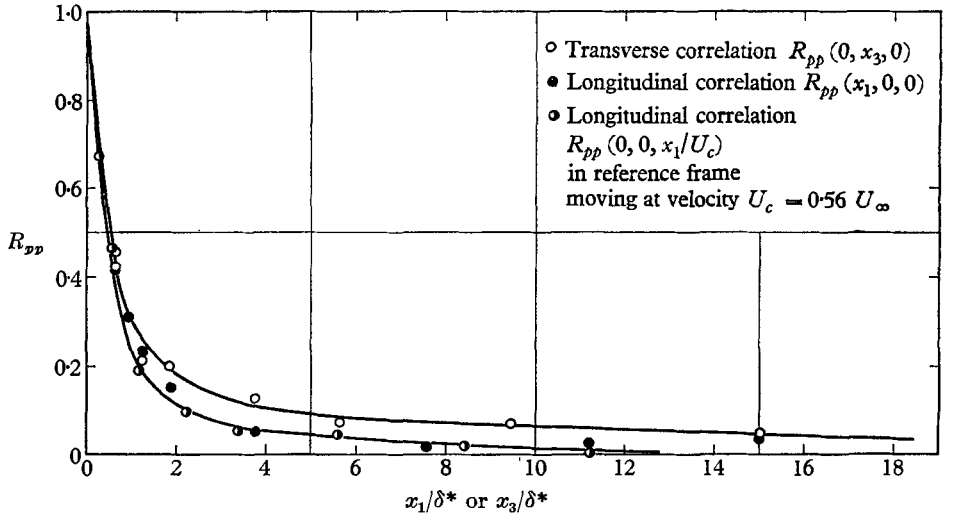

FIGURE 11. Transverse and longitudinal spatial correlation of the pressure produced by pressure fluctuations in the frequency band $105 < f < 10{,}000$ c/s.

6. Comparison of the transverse and longitudinal scale of the pressure fluctuations

Measurements of the transverse correlation of the pressure for various spatial separations of the transducers were also made in the frequency band from 105 to 10,000 c/s. The transverse correlation for a large or small transducer separation was found to be a maximum when the time delay was zero. All the transverse correlation measurements have been made with zero time delay.

The results of measurements with zero time delay of both the longitudinal pressure correlation $R_{pp}(x_1, 0,0)$ and the transverse correlation $R_{pp}(0, x_3, 0)$ are shown in figure 11. The approximate spatial correlation of the pressure in the stream direction that would be measured by an observer moving downstream at the convection speed $0{\cdot}56U_\infty$ is also shown in this figure. The correlation in a moving reference frame was obtained from the measured autocorrelation of the pressure, $R_{pp}(0, 0, \tau)$, of figure 5 with $\tau = x_1/U_c$. The measured autocorrelation of figure 5 was approximately corrected for the loss of the low-frequency

energy below 105 c/s that was rejected by the filter. The correction was made by assuming the power spectrum of the pressure below 105 c/s to be constant and equal to the value at 105 c/s.

The transverse and longitudinal pressure correlation data show that the spatial extent of the pressure correlation over the entire frequency band is approximately the same in directions parallel and transverse to the stream. Favre, Gaviglio & Dumas (1957) found the scale of the spatial correlation of the streamwise velocity fluctuations u to be much larger in the stream direction than in a direction transverse to the stream. Their result does not necessarily conflict with the present measurements of the scale of the wall-pressure fluctuations because Kraichnan (1956*b*) suggests that the dominant term in the

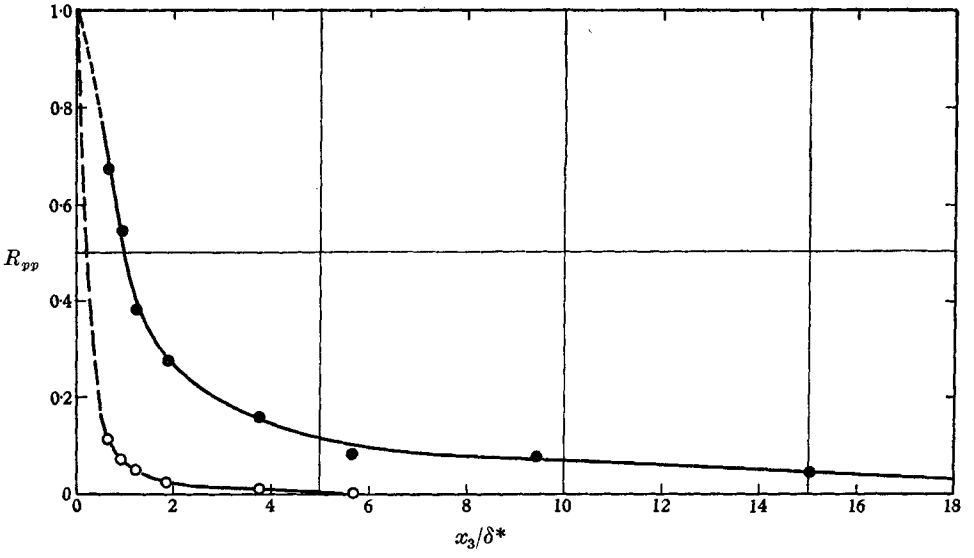

FIGURE 12. Transverse wall pressure correlations measured in a low- and a high-frequency band. ●, $300 < f < 700, 0{\cdot}41 < \omega\delta^*/U_\infty < 0{\cdot}95$; ○, $3000 < f < 5000, 4{\cdot}1 < \omega\delta^*/U_\infty < 6{\cdot}8$.

interaction between the turbulence and mean shear which produces the wall pressure is $\rho(\partial U/\partial y)(\partial v/\partial x)$. The spatial scale of the correlation of a velocity derivative in the direction of differentiation may be much less than the scale of the velocity correlation itself in the same direction.

The presence of sound waves of large wavelength, $\lambda \simeq 6$ ft., propagating upstream in the free stream may cause the spatial extent of the pressure correlation transverse and parallel to the stream to be overestimated at small values of the pressure correlation. The measurements of figure 11 therefore overestimate the spatial extent of the wall-pressure correlation for large values of x_1 or x_3 where $R_{pp} < 0{\cdot}1$, but are believed to be accurate for values of $R_{pp} > 0{\cdot}1$.

Measurements of the spatial correlation transverse to the stream produced by pressure fluctuations in a frequency band centred at low and high frequencies are shown in figure 12. The low-frequency band was chosen slightly above the frequency of the sound in the test section. The pressure correlations have been normalized by the value of the autocorrelation in the same frequency band. It

is apparent that the transverse scale of low-frequency pressure fluctuations is much larger than the transverse scale of the high-frequency pressure fluctuations.

A very crude comparison of the longitudinal and transverse scale of the eddies may easily be obtained. If the decay of the pressure at the convection speed is ignored, the transverse correlation measurements of figure 12 are produced by pressure-producing eddies that have a half wavelength in the stream direction of magnitude

$$\frac{\lambda}{2\delta^*} = \pi \frac{U_c}{U_\infty} \left(\frac{\overline{\omega}\delta^*}{U_\infty} \right)^{-1}. \tag{11}$$

For the low- and high-frequency band, the half wavelength turns out to be $\lambda/2\delta^* = 2{\cdot}8$ and $0{\cdot}4$, respectively. We may conclude from this and from figure 12 that the transverse and longitudinal scale of both the large and small pressure-producing eddies are of the same order of magnitude.

The authors wish to express their appreciation of many fruitful discussions with Professors A. M. Kuethe, E. G. Gilbert, M. S. Uberoi and C. S. Yih, and Mr J. L. Amick. The assistance of Mr R. Enlow and Mr H. Kristen who helped us obtain and evaluate the data is gratefully acknowledged. The investigation was supported by the Office of Naval Research under contract no. Nonr 1224 (30).

REFERENCES

BATCHELOR, G. K. 1950 *Proc. Camb. Phil. Soc.* **47**, 359.

BRADSHAW, P. & GREGORY, N. 1961 *Aero. Res. Counc., Lond., Rep. & Mem.* no. 3202.

BULL, M. K. 1960 *Dept. Aero. Astro., Univ. of Southampton, Rep.* no. 149.

BULL, M. K. & WILLIS, J. L. 1961 *Dept. Aero. Astro., Univ. of Southampton, Rep.* no. 199.

COLES, D. 1953 *Jet Propulsion Lab., Calif. Inst. Tech., Rep.* no. 20–69; or 1954 *Z.A.M.P.* **5**, 181.

CORCOS, G. M. 1959 *Amer. Phys. Soc., Div. of Fluid Dynamics, Abstracts.*

CORCOS, G. M. 1962 *Univ. of Calif., Inst. of Eng. Res. Rep., Series* 183, no. 1.

FAVRE, A. J., GAVIGLIO, J. J. & DUMAS, R. 1957 *J. Fluid Mech.* **2**, 313.

HARRISON, M. 1958 *Hydro. Lab., David Taylor Model Basin, Rep.* no. 1260.

KRAICHNAN, R. H. 1956*a* *J. Acoust. Soc. Amer.* **28**, 64.

KRAICHNAN, R. H. 1956*b* *J. Acoust. Soc. Amer.* **28**, 378.

LAUFER, J. 1961 *Jet Propulsion Lab., Calif. Inst. Tech., Tech. Rep.* pp. 32–119.

LILLEY, G. M. & HODGSON, T. H. 1960 *AGARD Rep.* no. 276.

PHILLIPS, O. M. 1957 *J. Fluid Mech.* **2**, 417.

SKUDRZYK, E. J. & HADDLE, G. P. 1960 *J. Acous. Soc. Amer.* **32**, 19.

UBEROI, M. S. 1953 *J. Aero. Sci.* **20**, 197.

WILLMARTH, W. W. 1958*a* *J. Aero. Sci.* **25**, 335.

WILLMARTH, W. W. 1958*b* *Rev. Sci. Inst.* **29**, 218.

WILLMARTH, W. W. 1959 NASA *Mem.* 3–17–59W.